Inorganic Chemistry
Article
pubs.acs.org/IC

From One to Three Dimensions: Corrugated $^{1}_{\infty}$[NiGe] Ribbons as a Building Block in Alkaline Earth Metal Ae/Ni/Ge Phases with Crystal Structure and Chemical Bonding in AeNiGe (Ae = Mg, Sr, Ba)

Viktor Hlukhyy, Lisa Siggelkow, and Thomas F. Fässler*

Department of Chemistry, Technische Universität München, Lichtenbergstr. 4, 85747 Garching, Germany

Supporting Information

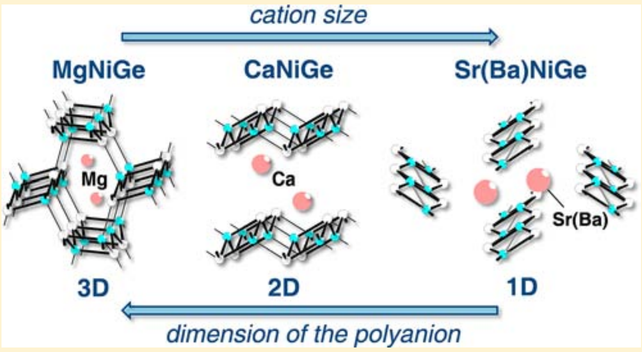

ABSTRACT: The new equiatomic nickel germanides MgNiGe, SrNiGe, and BaNiGe have been synthesized from the elements in sealed tantalum tubes using a high-frequency furnace. The compounds were investigated by X-ray diffraction both on powders and single crystals. MgNiGe crystallizes with TiNiSi-type structure, space group *Pnma*, $Z = 4$, $a = 6.4742(2)$ Å, $b = 4.0716(1)$ Å, $c = 6.9426(2)$ Å, $wR_2 = 0.033$, 305 F^2 values, 20 variable parameters. SrNiGe and BaNiGe are isotypic and crystallize with anti-SnFCl-type structure ($Z = 4$, *Pnma*) with $a = 5.727(1)$ Å, $b = 4.174(1)$ Å, $c = 11.400(3)$ Å, $wR_2 = 0.078$, 354 F^2 values, 20 variable parameters for SrNiGe, and $a = 5.969(4)$ Å, $b = 4.195(1)$ Å, $c = 11.993(5)$ Å, $wR_2 = 0.048$, 393 F^2 values, 20 variable parameters for BaNiGe. The increase of the cation size leads to a reduction of the dimensionality of the [NiGe] polyanions. In the MgNiGe structure the nickel and germanium atoms build a $^{3}_{\infty}$[NiGe] network with magnesium atoms in the channels. In SrNiGe and BaNiGe the $^{1}_{\infty}$[NiGe] ribbons are separated by strontium/barium atoms, whereas in the known CaNiGe structure the ribbons are fused to two-dimmensional atom slabs. The crystal chemistry and chemical bonding in AeNiGe (Ae = Mg, Ca, Sr, Ba) are discussed. The experimental results are reconciled with electronic structure calculations performed using the tight-binding linear muffin-tin orbital (TB-LMTO-ASA) method.

■ INTRODUCTION

The Zintl−Klemm concept provides a universal way to describe the relationship between crystal structure and chemical bonding in a large variety of intermetallic compounds containing electropositive metals such as alkali (A) or alkaline earth (Ae) metals and a p-block (semi)metal (E).[1] Localized chemical bonding pictures predict the connectivity of the polyanions consisting of p-block atoms E according to the valence rules. Similar to $[E_n]^{m-}$ polyanions in Zintl phases, specific atom arrangements $[T_pE_n]^{m-}$ recurrently occur in ternary polar intermetallic phases containing additional transition metals (T). Even though metallic properties are expected from the corresponding band structures, a *formal* electron transfer from the A or Ae atoms leads in the case of ternary $A_mT_pE_n$ and $Ae_{m/2}T_pE_n$ intermetallic compounds formally to polyanionic units $[T_pE_n]^{m-}$.

Unlike Zintl phases, polar intermetallic compounds show more delocalized chemical bonding in their polyanionic networks compared to the classical 2c−2e chemical bonds. However, like in Zintl phases, increasing amounts of Ae lead to a reduction of the dimensionality of the polyanionic $[Ni_pGe_n]^{m-}$ structures in the polar intermetallic phases $Ae_{m/2}Ni_pGe_n$. The $[Ni_pGe_n]^{m-}$ substructures in alkaline earth nickel germanides usually occur as three-dimensional polyanionic networks (in $MgNi_6Ge_6$, $Mg_6Ni_{16}Ge_7$, $CaNi_2Ge_2$, $CaNi_5Ge_3$, $CaNiGe_3$, $CaNiGe_2$, $Ca_7Ni_{49}Ge_{22}$, $Ca_{15}Ni_{68}Ge_{37}$, $Ca_5Ni_{17}Ge_8$, $SrNi_2Ge_2$, $SrNiGe_2$, $SrNiGe_3$, $Ba_8Ni_{3.5}Ge_{42.1}$)[2−10] or as two-dimensional Ni−Ge polyanionic layers (in CaNiGe, $Ca_2Ni_3Ge_2$, $Ca_4Ni_4Ge_3$, $SrNi_3Ge_2$, $SrNi_2Ge$, $BaNi_2Ge$, $Ba_2Ni_5Ge_4$, $BaNi_2Ge_2$),[11−16] and a reduction of the dimensions of the $[Ni_pGe_n]^{2m-}$ substructures is observed with an increase of the alkaline earth metal content.

We further studied the influence of the size of the Ae atoms on the type and dimensionality of the Ni−Ge polyanions in a series of equiatomic compounds AeNiGe (Ae = Mg, Ca, Sr, and Ba). The recently reported CaNiGe crystallizes in the well-known CeFeSi type with PbO-like $^{2}_{\infty}$[NiGe] layers.[11] The alteration of CaNiGe through Mn/Ni substitution or hydrogenation does not significantly change the square lattice topology of the TGe layer; however, it has an influence on the electric and magnetic properties.[17,18] Here we report on the alkaline earth metal-substituted phases SrNiGe and BaNiGe, which show unique one-dimensional $^{1}_{\infty}$[NiGe] ribbons in the crystal, and on MgNiGe, in which a three-dimensional $^{3}_{\infty}$[NiGe] network with exclusively four-bonded Ni and Ge atoms appears as polyanionic substructure. Calculations of the electronic structure including the analysis of the band structure,

Received: December 6, 2012
Published: June 6, 2013

dx.doi.org/10.1021/ic302681t | *Inorg. Chem.* 2013, 52, 6905−6915

Table 1. Crystal Data and Structure Refinement for MgNiGe, SrNiGe, and BaNiGe (Space Group *Pnma*, $Z = 4$)

	MgNiGe	SrNiGe	BaNiGe
M_w, g mol^{-1}	155.61	218.92	268.64
unit cell params (powder data)			
a, Å	6.4742(2)	5.727(1)	5.969(4)
b, Å	4.0716(1)	4.174(1)	4.195(1)
c, Å	6.9426(2)	11.400(3)	11.993(5)
V, Å^3	183.01(1)	272.5(1)	300.3(2)
μ (Mo Kα), mm^{-1}	26.5	36.9	28.8
ρ_{calcd}, g cm^{-3}	5.65	5.34	5.94
diffractometer	Oxford-Xcalibur3	Stoe IPDS-2T	Stoe IPDS-2T
cryst size (mm^3)	0.04 × 0.07 × 0.09	0.01 × 0.02 × 0.08	0.01 × 0.02 × 0.06
$F(000)$	288	392	464
θ range for data collection (deg)	3−30	5−27	2−32
range in h,k,l	$-9 \le h \le 8$, $-5 \le k \le 4$, ±9	±7, ±5, ±14	±7, ±5, ±15
reflns collected	1556	4201	4590
indep reflns (R_{int})	305 (0.016)	358 (0.110)	393 (0.061)
reflns with $I > 2\,\sigma(I)$ (R_σ)	294 (0.010)	298 (0.040)	354 (0.021)
data/params	305/20	358/20	393/20
GOF on F^2	1.298	1.057	1.077
R_1, wR_2 [$I > 2\sigma(I)$]	0.015, 0.033	0.036, 0.078	0.022, 0.048
R_1, wR_2 (all data)[a,b]	0.015, 0.033	0.048, 0.082	0.027, 0.049
extinction coeff	0.026(2)	0.003(1)	0.0024(5)
largest diff peak and hole (e Å^{-3})	0.58 and −0.65	1.04 and −1.08	1.97 and −0.92

[a] $R_1 = \Sigma||F_c| - |F_c||/\Sigma|F_o|$; $wR_2 = [\Sigma[w(F_o^2 - F_c^2)^2]/\Sigma[w(F_o^2)^2]]^{1/2}$. [b] $w = 1/[\sigma^2(F_o^2) + (aP)^2 + bP]$, where $P = (\mathrm{Max}(F_o^2,0) + 2F_c^2)/3$.

the COHP, and the ELF for an analysis of the chemical bonding complement the experimental findings.

EXPERIMENTAL SECTION

Synthesis. Starting materials for the synthesis of MgNiGe, SrNiGe, and BaNiGe were ingots of magnesium (ChemPur), strontium (ChemPur), and barium (ChemPur), nickel wire (⌀ 1 mm, Johnson-Matthey), and germanium pieces (ChemPur), all with stated purities better than 99.5%. Pieces of the alkaline earth metals, pieces of nickel wire, and pieces of germanium were mixed in a 1:1:1 atomic ratio. The mixtures were subsequently sealed in tantalum tubes under argon atmosphere (Mini Arc Melting System, MAM-1, Johanna Otto GmbH, placed in an argon filled glovebox). The crucibles were placed in a water-cooled sample chamber of an induction furnace (Hüttinger Elektronik, Freiburg, Typ TIG 2.5/300), heated under flowing argon up to approximately 950 °C and kept at that temperature for 30 min. The exothermic character of the reaction between the elements was manifested through a slight flash of light. After the melting procedure the samples were cooled within one hour to approximately 600 °C, kept at that temperature for another hour, and finally quenched to room temperature by switching off the furnace. The temperature above 900 °C was controlled through a Sensor Therm Metis MS09 pyrometer with an accuracy of ±10 K. After cooling to room temperature, the gray samples could easily be separated from the tantalum crucibles. No reactions of the samples with the crucible material could be detected. The MgNiGe sample is stable in moist air as finely grained powder, whereas the powdered samples of SrNiGe and BaNiGe are stable under these conditions only for a few days. Good-quality irregularly shaped crystals in the case of MgNiGe and needle-like crystals in the cases of SrNiGe and BaNiGe with metallic luster were isolated from the crushed samples. The synthesis of SrNiGe and BaNiGe can easily be reproduced by the arc melting technique (Mini Arc Melting System, MAM-1, Johanna Otto GmbH, placed in an argon-filled glovebox), whereas the synthesis of MgNiGe can only by carried out in welded Ta/Nb ampules due to the high vapor pressure of Mg.

X-ray Investigations. The purity of the sample was checked using a Stoe STADI P powder diffractometer with Ge-monochromatized Cu Kα radiation (λ = 1.54056 Å). The orthorhombic lattice parameters (Table 1) were obtained from least-squares fits of the powder data of MgNiGe, SrNiGe, and BaNiGe. The correct indexing of the patterns was ensured through intensity calculations taking the atomic positions from the structure refinements obtained from single-crystal X-ray diffraction measurements. In all cases the lattice parameters determined from powder patterns and from single-crystal data agreed well. The Rietveld refinement with the Fullprof suite[19] showed that the sample of MgNiGe contained about 4% of Mg_2Ge[20] and 7% $MgNi_6Ge_6$,[2] whereas SrNiGe and BaNiGe were obtained as single-phase products within the accuracy of the powder diffraction method (Supporting Information, Figures S1−S3).

A single crystal of MgNiGe was measured at room temperature on an Oxford-Xcalibur3 diffractometer (CCD area detector) with graphite-monochromatized Mo Kα (λ = 0.710 73 Å) radiation. Single-crystal data of SrNiGe and BaNiGe were collected in the ϕ scan mode using a Stoe IPDS-IIT imaging plate detector diffractometer (Mo Kα radiation, λ = 0.710 73 Å, graphite monochromator) at room temperature. Numerical absorption corrections with optimized crystal shapes using the X-SHAPE and X-RED programs (X-Shape/X-Red)[21,22] were performed for SrNiGe and BaNiGe, whereas for MgNiGe the absorption was corrected empirically.[23] All structures were solved using direct methods (SHELXS)[24] and refined by full-matrix least-squares using SHELXL.[25] Direct methods provided the positions of atoms in the orthorhombic primitive space group *Pnma*. The occupation factors of all atoms did not deviate from unity. All final cycles included anisotropic displacement parameters and revealed no significant residual peaks. All relevant crystallographic data for the data collection and evaluation are listed in Table 1. Final atomic positions with equivalent displacement parameters are given in Table 2 and selected bond lengths in Table 3.

After data collection the single crystals were analyzed by EDX measurements with a Jeol SEM 5900LV scanning electron microscope equipped with an Oxford Instruments INCA energy dispersive X-ray microanalysis system. No impurity elements heavier than sodium have been observed. The analysis of well-shaped single crystals has revealed the following compositions (in atomic percentages): Mg 27(3), Ni 36(4), and Ge 37(5) for MgNiGe; Sr 29(3), Ni 36(5), and Ge 35(5) for SrNiGe; and Ba 36(4), Ni 33(4), and Ge 31(5) for BaNiGe. These

Table 2. Atomic Coordinates and Equivalent Isotropic Displacement Parameters ($Å^2 \times 10^3$) for MgNiGe, SrNiGe, and BaNiGe[a]

atom	Wyckoff position	x	y	z	U_{eq}
		MgNiGe			
Mg	4*c*	0.0019(2)	$^1/_4$	0.6876(2)	11.6(2)
Ni	4*c*	0.34605(6)	$^1/_4$	0.44589(5)	10.4(1)
Ge	4*c*	0.21043(5)	$^1/_4$	0.11862(4)	9.5(1)
		SrNiGe			
Sr	4*c*	0.1194(2)	$^1/_4$	0.35634(9)	25.7(3)
Ni	4*c*	0.1006(2)	$^1/_4$	0.0441(1)	23.0(4)
Ge	4*c*	0.3646(2)	$^1/_4$	0.6288(1)	25.3(3)
		BaNiGe			
Ba	4*c*	0.11787(7)	$^1/_4$	0.35200(3)	21.3(2)
Ni	4*c*	0.0960(2)	$^1/_4$	0.04111(7)	18.6(2)
Ge	4*c*	0.3690(1)	$^1/_4$	0.62128(6)	19.6(2)

[a] U_{eq} is defined as one third of the trace of the orthogonalized U_{ij} tensor.

values are within the standard deviations in agreement with the ideal equiatomic compositions.

Magnetic Susceptibility Measurements. Direct current (DC) magnetization data were collected using a Quantum Design MPMS XL5 superconducting quantum interference device (SQUID). The temperature-dependent data were obtained by measurement of the magnetization from 1.8 to 300 K in an applied magnetic field of 5 kOe and 1 kOe for BaNiGe and SrNiGe, respectively, by using the powdered samples fixed in a calibrated gelatin capsule and kept at the center of a drinking straw. The temperature-dependent measurements were performed under zero-field-cooled (ZFC) and field-cooled (FC) conditions in an applied magnetic field of 50 Oe.

Electronic Structure Calculations. The electronic structures were investigated by means of the *ab initio* linear muffin-tin orbital (LMTO) method in the atomic sphere approximation (ASA) using the tight-binding (TB) program TB-LMTO-ASA.[26] The basis set of short-range atom-centered TB-LMTOs contained s−p valence functions for Mg, s−f valence functions for Sr and Ba, and s−d valence functions for Ni and Ge. Mg 3p; Sr 5p, 4f; Ba 6p; and Ge 3d orbitals were included using a downfolding technique.[27,28] To achieve space filling within the atomic sphere approximation, interstitial spheres were introduced to avoid too large overlap of the atom-centered spheres. The empty sphere positions and radii were calculated using an automatic procedure. We did not allow an overlap of more than 16% for any two atom-centered spheres. In the fatband analysis the atomic orbital character is represented as a function of the bandwidth. For analyzing the band structure of MgNiGe, SrNiGe, and BaNiGe the following *k*-path has been chosen: Γ = (0, 0, 0), Z = (0, 0, $^1/_2$), T = (0, $^1/_2$, $^1/_2$), Y = (0, $^1/_2$, 0), Γ = (0, 0, 0), X = ($^1/_2$, 0, 0), S = ($^1/_2$, $^1/_2$, 0), R = ($^1/_2$, $^1/_2$, $^1/_2$), and U = ($^1/_2$, 0, $^1/_2$). The total and partial densities-of-states (DOS) were computed. The crystal orbital Hamilton populations (COHPs) were employed for an analysis of the chemical bonding.[29] From COHP analyses, the contribution of the covalent part of a particular interaction to the total bonding energy of the crystal can be obtained. All COHP curves are presented in the following format: positive regions indicate bonding, and negative regions show antibonding interactions. The Fermi level E_F was set as a reference point at 0 eV.

RESULTS AND DISCUSSION

Description of the Crystal Structures. Like other equiatomic germanides and silicides,[30,31] MgNiGe crystallizes with the well-known TiNiSi-type structure (AlB_2-type derivative, space group *Pnma*). The structural relationships between 46 structure types derived from the AlB_2 system have been discussed on the basis of a group−subgroup scheme.[32] In

Table 3. Interatomic Distances (Å), Calculated with the Lattice Parameters Taken from the Powder X-ray Data and Corresponding Integrated Crystal Orbital Hamilton Populations (−iCOHPs) Values at E_F of MgNiGe, SrNiGe, and BaNiGe

		distance (Å)	−iCOHP (eV/bond)			distance (Å)	−iCOHP (eV/bond)
				MgNiGe			
Ni−	Ge	2.391(1) (2 ×)	2.13	Mg−	Ni	2.737(2) (1 ×)	0.67
	Ge	2.401(1) (1 ×)	2.00		Ni	2.789(2) (1 ×)	0.84
	Ge	2.436(1) (1 ×)	2.22		Ge	2.800(1) (2 ×)	0.72
					Ge	2.801(1) (2 ×)	0.68
Ge−	Ni	2.391(1) (2 ×)	2.13		Ge	2.843(2) (1 ×)	0.70
	Ni	2.401(1) (1 ×)	2.00		Ni	2.886(1) (2 ×)	0.62
	Ni	2.436(1) (1 ×)	2.22		Ge	3.283(1) (2 ×)	0.32
				SrNiGe			
Ni−	Ge	2.308(2) (2 ×)	2.95	Sr−	Ni	2.980(2) (1 ×)	0.46
	Ge	2.390(2) (1 ×)	2.11		Ni	3.180(2) (1 ×)	0.47
	Ni	2.588(2) (2 ×)	1.10		Ge	3.331(2) (2 ×)	0.55
					Ni	3.393(2) (2 ×)	0.28
Ge	Ni	2.308(2) (2 ×)	2.95		Ge	3.409(2) (1 ×)	0.30
	Ni	2.390(2) (1 ×)	2.11		Ge	3.474(2) (2 ×)	0.36
					Ni	3.561(2) (1 ×)	0.22
					Ge	3.622(2) (2 ×)	0.24
				BaNiGe			
Ni−	Ge	2.317(1) (2 ×)	2.97	Ba−	Ni	3.129(2) (1 ×)	0.49
	Ge	2.372(2) (1 ×)	2.26		Ni	3.369(3) (1 ×)	0.45
	Ni	2.585(2) (2 ×)	1.13		Ge	3.473(2) (2 ×)	0.56
					Ni	3.530(2) (2 ×)	0.29
Ge−	Ni	2.317(1) (2 ×)	2.97		Ge	3.560(2) (1 ×)	0.29
	Ni	2.372(2) (1 ×)	2.26		Ge	3.598(2) (2 ×)	0.37
					Ge	3.726(2) (2 ×)	0.26
					Ni	3.732(2) (1 ×)	0.22

analogy to boron nitride the structure of MgNiGe is derived from the well-known aristotype AlB_2 via an ordering of the Ni and Ge atoms on the graphite-type boron layer of AlB_2. The 6^3 nets parallel to the *bc* plane are strongly puckered, and heteroatomic bonds are formed in between the layers.

The resulting three-dimensional NiGe network with alternating Ni and Ge atoms consists of four-, six-, and eight-membered Ni–Ge polygons. The largest eight-membered polygons form channels along the *b* axis, which are occupied with Mg atoms (Figure 1a). The Ni–Ge distances range from 2.391(1) to 2.436(1) Å and compare well to the sum of Pauling's single bond radii of 2.44 Å.[33] There are no close Ni–Ni and Ge–Ge contacts within the $^{3}_{\infty}$[NiGe] network. All atoms of the network are four connected to neighboring atoms with strongly distorted tetrahedral coordination. The Ni–Ge–Ni and Ge–Ni–Ge bond angles range from 75.89(2)° to 121.88(2)° and from 100.38(2)° to 116.74(2)°, respectively. In the case of Ge leads the distortion to trigonal pyramids of neighboring Ni atoms, with the centering Ge atoms situated close to the basal plane. Each Mg atom in MgNiGe has 12 nearest Ni/Ge neighbors with distances ranging from 2.737(1) to 3.283(1) Å; the resulting Ni_6Ge_6 coordination polyhedron can be described as a distorted hexagonal prism.

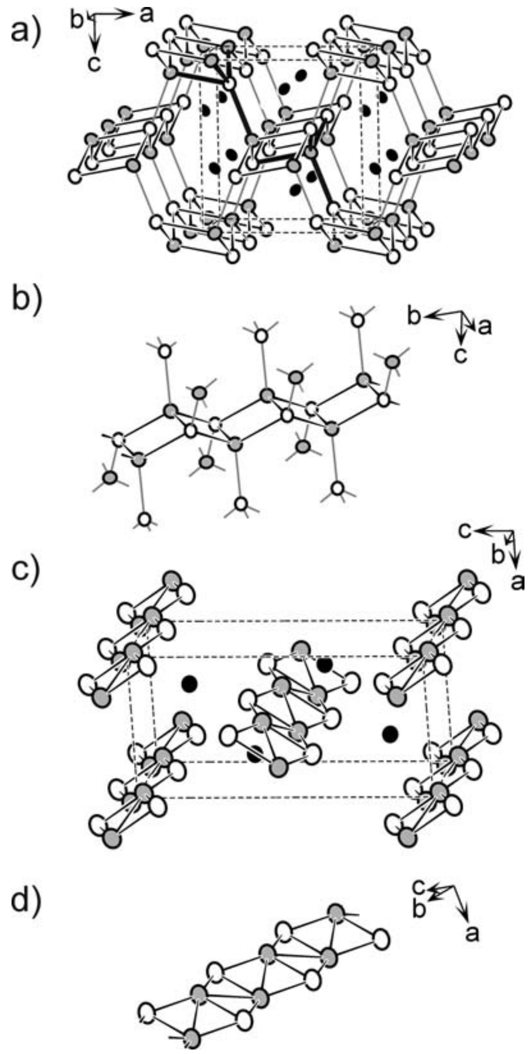

Figure 1. View of the MgNiGe (a) and BaNiGe (c) structures approximately along the *b* axis. The $^{3}_{\infty}$[NiGe] network of MgNiGe as well as $^{1}_{\infty}$[NiGe] ribbons of BaNiGe are emphasized. For MgNiGe the coordination environment of Ni and Ge is emphasized. A closer look on the $^{1}_{\infty}$[NiGe] substructures is given for MgNiGe (b) and for BaNiGe (d). The Mg (Ba) atoms are drawn as black spheres, and Ni and Ge atoms as gray and white ones, respectively. The displacement ellipsoids are drawn at the 90% probability level.

Due to the puckering of the [NiGe] layers based on AlB_2-type structure and due to the orthorhombic distortion of the [NiGe] polyanions with formation of relatively short interlayer Ni–Ge bonds, [NiGe] ribbons emerge (Figure 1a,b). In the Ni_2Ge_2 rhombic units of the ribbons the more electronegative Ge atoms occupy positions with maximum Ge–Ge distances (minimum repulsion), and thus the Ge–Ge distance of 3.779(1) Å is significantly longer than the Ni–Ni distance of 2.946(1) Å. Such trend of a tilting of T_2X_2 units was recently discussed for different representatives of the TiNiSi-type structure, which proved to be flexible against the exchange of atoms.[34,35] An organic analogue of an isolated $^{1}_{\infty}[Ni_2Ge_2]$ ribbon is the cyclobutane ladder polymer, and the ladder polysilanes $\text{-}(Si_2R_2)_n\text{-}$ have been studied theoretically by density functional theory.[36]

In order to be able to compare the MgNiGe structure with the forthcoming AeNiGe structures the two-atom wide $^{1}_{\infty}[Ni_2Ge_2]$ zigzag ribbon with d(Ni–Ge) = 2.391(1) Å and 2.401(1) Å is emphasized in Figure 1a,b. The rhombic Ni_2Ge_2 units are interconnected along the *b* direction to a ladder structure ($^{1}_{\infty}[Ni_2Ge_2]$ ribbons) with a dihedral angle α between the rhombic Ni_2Ge_2 units of 122.80(2)° (Figure 1a,b, Table 4, Scheme 1). These ribbons are further interconnected through slightly longer Ni–Ge bonds (2.436(1) Å) to a three-dimensional network.

SrNiGe and BaNiGe are the first representatives of intermetallic compounds that crystallize with the anti-SnClF-type structure (space group *Pnma*). Their crystal structure consists of unique one-dimensional two-atom wide zigzag $^{1}_{\infty}$[NiGe] ribbons running along the *b* axis and being separated by Sr and Ba atoms (Figure 1c). These $^{1}_{\infty}$[NiGe] ribbons are similar to those described above for MgNiGe. They consist of rhombic Ni_2Ge_2 units, which are interconnected along *b* via Ni–Ge bonds into a ladder structure.

The observed Ni–Ge distances within the $^{1}_{\infty}$[NiGe] ribbons (2 × 2.308(1) Å and 1 × 2.390(2) Å for SrNiGe as well as 2 × 2.317(1) Å and 1 × 2.372(2) Å for BaNiGe, Table 3) are shorter than the Pauling single bond distances (2.44 Å) but comparable to those of other Ae/Ni/Ge (Ae = alkaline earth metals) compounds, such as $Ba_2Ni_5Ge_4$ (shortest Ni–Ge contact of 2.291 Å),[15] $Ca_5Ni_{17}Ge_8$ (2.335 Å),[8] $CaNiGe_2$ (2.341 Å),[7] $Ca_2Ni_3Ge_2$ (2.346 Å).[12] The rhombic distortion from a Ni_2Ge_2 square is more pronounced in the Sr- and Ba-containing compounds compared to the intermetallic phase MgNiGe, expressed by the deviation of the Ni–Ge–Ni angle from 90° (MgNiGe, 75.88(2)°; SrNiGe, 66.83(5)°; BaNiGe, 66.91(2)°). As a result additional Ni–Ni bonds with a length of 2.588(2) and 2.585(2) Å for SrNiGe and BaNiGe, respectively (in contrast to d(Ni–Ni) = 2.946(1) Å for MgNiGe), are formed, and zigzag Ni chains within the polymeric $^{1}_{\infty}$[NiGe] ribbons appear (Figure 1d). In comparison to fcc nickel (2.49 Å),[33] the Ni–Ni distances in Sr(Ba)NiGe are elongated. Consequently, the zigzag ribbon (ladder structure) is flattened compared to that of MgNiGe, as is expressed by the increase of the dihedral angle α (Sheme 1, Table 4). For SrNiGe and BaNiGe, dihedral angles of 159.30(7)° and 159.60(5)°, respectively, result.

Table 4. Inter- and Intraribbon Ni–Ge and Ni–Ni Distances and the Angle of the Ladder Structure of MgNiGe, CaNiGe, SrNiGe, BaNiGe, $Ca_4Ni_4Ge_3$, $SrNi_2Ge$, $BaNi_2Ge$, and $SrNi_3Ge_2$

	d(Ni–Ge) intraribbon /Å	d(Ni–Ge) inter-ribbon /Å	d(Ni–Ni) intraribbon /Å	d(Ni–Ni) inter-ribbon /Å	α[a] /deg
MgNiGe	2.391(1)	2.436(1)	2.947(1)		122.80(2)
	2.401(1)				
CaNiGe	2.433	2.433	2.965	2.965	126.20
SrNiGe	2.308(1)		2.588(2)		159.30(7)
	2.390(2)				
BaNiGe	2.317(1)		2.586(2)		159.60(5)
	2.372(2)				
$Ca_4Ni_4Ge_3$	2.407	2.451[b]	2.526	2.487	151.90
	2.416				
$SrNi_2Ge$	2.409	2.409[c]	2.485	2.484[c]	151.69
$BaNi_2Ge$	2.422	2.422[c]	2.533	2.483[c]	150.03
	2.428	2.428[c]			
$SrNi_3Ge_2$	2.395	2.362	3.121	3.121	120.00
	2.362	2.706[d]		2.557[d]	

[a] Dihedral angle α of the ladder structure (see Scheme 1). [b] Distance ribbon–(Ni–Ge–Ni) bridge, see Figure 3d. [c] Distance ribbon–Ni chain, see Figure 3e,f. [d] Distance ribbon–Ni atom, see Figure 3g.

Scheme 1. Ladder ${}^{1}_{\infty}[\mathrm{NiGe}]$[a]

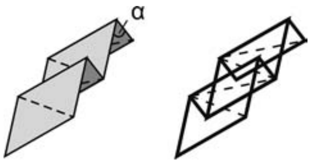

[a] The Ni–Ni bonds are shown as dashed lines, the dihedral angle α is given in Table 4.

The Ni–Ge and Ni–Ni distances within the ${}^{1}_{\infty}[\mathrm{NiGe}]$ ribbon are only slightly affected by the nature of the Ae atoms (Ae = Sr, Ba). This is also reflected by the values of the unit cell parameters of SrNiGe and BaNiGe: while the parameters *a* and *c*, which determine the inter-ribbon contacts, are increased by 4.2% and 5.2%, respectively, the parameter *b* that measures the length of ${}^{1}_{\infty}[\mathrm{NiGe}]$ ribbons, changes only slightly (0.5%). This anisotropic behavior is a strong indication that Ni–Ge bonds play a dominant role. This strong interaction within the ${}^{1}_{\infty}[\mathrm{NiGe}]$ ribbons underlines their polyanionic character.

The coordination sphere of the nickel atoms within the polyanions can be described as a $Ni_2\square Ge_3$ hexagon with one vacant Ni position in comparison to those of recently published $SrNi_2Ge$[14] and $BaNi_2Ge$;[13] i.e., each nickel atom has three germanium and two nickel neighbors in an almost planar coordination. Furthermore, each nickel atom has five nearest

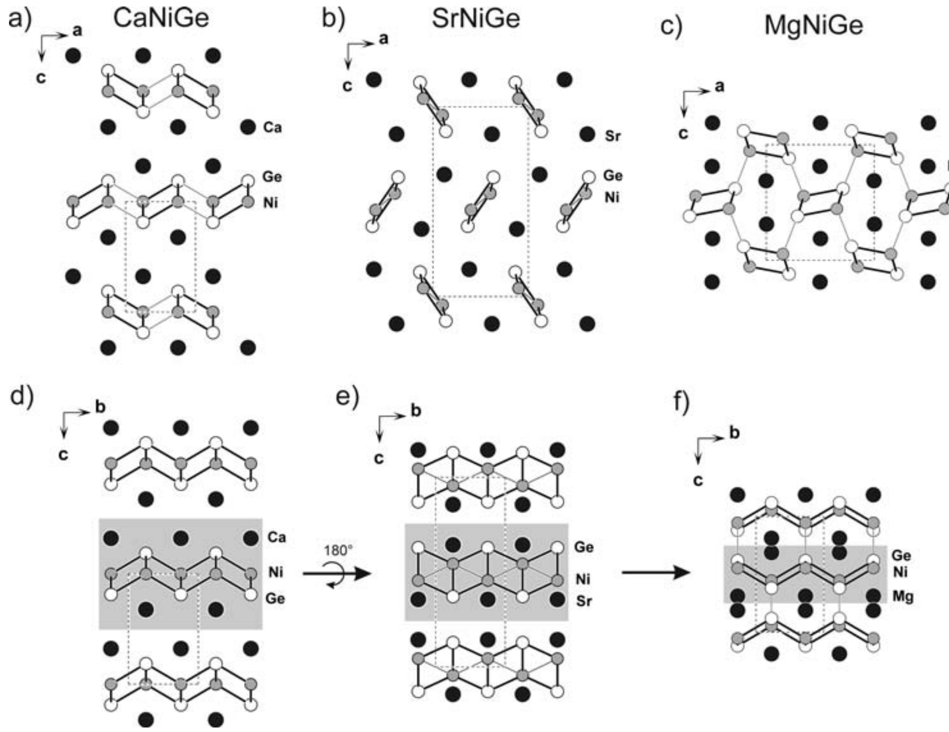

Figure 2. Topological relationships between the structures of CaNiGe (a, d), SrNiGe (b, e), and MgNiGe (c, f). The common [AeNiGe] slabs are highlighted to show the structural relationships.

Sr(Ba) neighbors, two above and three below the defect hexagon. Each Ge atom is coordinated by three Ni and seven Sr(Ba) atoms, and each Sr(Ba) atom by in total 12 atoms (five Ni and seven Ge). There are no close Ge−Ge contacts within the Sr(Ba)NiGe structure.

Structural Relationships. Comparative studies of the structure of intermetallic germanides Ae/Ni/Ge reveal that in many cases $^{1}_{\infty}$[NiGe] ribbons constitute the building block of $[\mathrm{Ni}_p\mathrm{Ge}_n]^{m-}$ polyanionic substructures. The three title structures nicely flank the known CaNiGe structure[11] with its $^{2}_{\infty}$[NiGe] substructure. This PbO-type $^{2}_{\infty}$[NiGe] layer can be interpreted as parallel-aligned $^{1}_{\infty}$[NiGe] ribbons which are interconnected perpendicular to their running direction. As the inter- and intraribbon Ni−Ge distances are equal, this remains a topological model. However, it allows uncovering structural relationships. As mentioned above, MgNiGe and Sr(Ba)NiGe crystallize in the same space group *Pnma* and are isopointal. Although the crystal structures of CaNiGe (*P4/nmm*) and Mg(Sr,Ba)NiGe (*Pnma*) are not directly related via a group−subgroup scheme, they are related in an interesting way: In CaNiGe the [AeNiGe] slabs are stacked along *c* in a primitive fashion, whereas in MgNiGe or Sr(Ba)NiGe these slabs are shifted by [0, $^1/_2$] in the *ab* plane (or turned by 180°) with respect to each other, as shown in Figure 2. This shift is accompanied by a strong uncoupling of the atomic coordinates leading to a reorganization of the covalent bonds within the [NiGe] substructure: breaking of several Ni−Ge bonds within the square $^{2}_{\infty}$[NiGe] net of CaNiGe along the *a* direction leads to the formation of $^{1}_{\infty}$[NiGe] ribbons, which are isolated in the case of Sr(Ba)NiGe or linked along the *c* direction via Ni−Ge bonds to a 3D network in MgNiGe.

Thus, the three Ni−Ge partial structures (Figure 3a−c) can be traced back to the same type of corrugated $^{1}_{\infty}$[NiGe] ribbons. These ribbons build a three-dimensional framework in MgNiGe and a puckered layer in the tetragonal CaNiGe structure, and they appear as isolated one-dimensional ribbons in SrNiGe and BaNiGe. In the same order, the ladder structure is flattened (the dihedral angles rise from 122.80(2)° in MgNiGe, to 126.20(1)° in CaNiGe, to 159.30(7)° and 159.60(5)° in SrNiGe and BaNiGe, respectively). The intraribbon Ni−Ni bonds remains almost unchanged when going from MgNiGe to CaNiGe (2.947(1) and 2.965(1) Å, respectively) but are drastically shortened in SrNiGe and BaNiGe (2.586(2) and 2.588(2) Å, respectively). Thus, the decrease of the dimensionality leads to a flattening of the ladder structure accompanied by the formation of Ni−Ni bonds.

As has been discussed above, the coordination polyhedra of nickel and germanium atoms in MgNiGe are strongly distorted tetrahedra. In CaNiGe the Ni atoms are tetrahedrally coordinated (angles (Ge−Ni−Ge) = 104.9−119.0°), and the Ge atoms have an umbrella-type coordination (angles (Ni−Ge−Ni) = 75°). In SrNiGe and BaNiGe the coordination number of Ni and Ge within the $^{1}_{\infty}$[NiGe] ribbon is reduced to three; however, the Ni atoms form additional Ni−Ni bonds along the diagonal of the rhomb (Figure 3c).

Interestingly, the Ni−Ge substructure of other recently described nickel germanides can also be traced back to corrugated $^{1}_{\infty}$[NiGe] ribbons. For example, the polar intermetallic compound $\mathrm{Ca_4Ni_4Ge_3}$ contains $^{2}_{\infty}[\mathrm{Ni_4Ge_3}]$ layers.[13] These can be described as being built up of $^{1}_{\infty}$[NiGe] ribbons (with a dihedral angle of 151.90°), which are interconnected by Ni−Ge−Ni bridges, as shown in Figure 3d. The $^{2}_{\infty}[\mathrm{Ni_2Ge}]$ layers of $\mathrm{SrNi_2Ge}$ and $\mathrm{BaNi_2Ge}$ are composed of corrugated Ge-centered Ni hexagons with chair (like gray arsenic) and boat (like graphane nets)[37] conformation, respectively. However, the layer can also be described as consisting of $^{1}_{\infty}$[NiGe] ribbons that are interconnected by parallel-oriented Ni zigzag chains (Figure 3e,f, respectively).[13,14] The polar intermetallic compound $\mathrm{SrNi_3Ge_2}$ contains $^{2}_{\infty}[\mathrm{Ni_3Ge_2}]$ slabs of condensed hexagonal Ni-centered prisms.[14] These can also be described as $^{1}_{\infty}$[NiGe] ribbons that now correspond to the prism heights, and the parallel-oriented ribbons are connected by Ni atoms (Figure 3g).

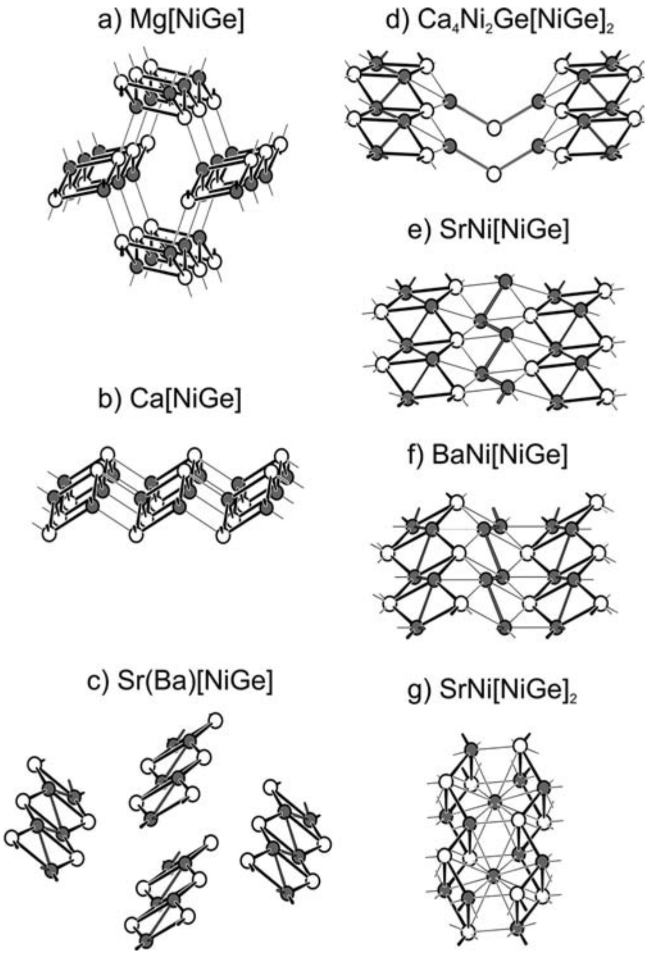

Figure 3. Ni−Ge substructures of MgNiGe (a), CaNiGe (b), Sr(Ba)NiGe (c), $\mathrm{Ca_4Ni_4Ge_3}$ (d), $\mathrm{SrNi_2Ge}$ (e), $\mathrm{BaNi_2Ge}$ (f), and $\mathrm{SrNi_3Ge_2}$ (g) containing similar $^{1}_{\infty}$[NiGe] ribbons (emphasized). The Ni and Ge atoms are drawn in gray and white, respectively.

In all these structures with $^{1}_{\infty}$[NiGe] ribbons as building blocks one interesting relation is observed: a flattening of the ribbons' corrugation (increasing of the dihedral angle α between fused $\mathrm{Ni_2Ge_2}$ rombs) leads to the formation of additional Ni−Ni bonds within the rombs although the Ni−Ge distances within the ribbons remain almost unchanged (see Table 4).

Further, the structures of $\mathrm{AeNi_2Ge_2}$ (Ae = Ca, Sr, Ba) contain [NiGe] layers similar to those found in CaNiGe and, consequently, are built up of $^{1}_{\infty}$[NiGe] ribbons.[4,16] These $^{1}_{\infty}$[NiGe] ribbons are also found in the structures of the recently published Ni-rich germanides $\mathrm{CaNi_5Ge_3}$, $\mathrm{Ca_{15}Ni_{68}Ge_{37}}$, and $\mathrm{Ca_7Ni_{49}Ge_{22}}$.[5] These ribbons are highly condensed and represent sections of the distorted $\mathrm{Ni_3Ge}$ structure.

In a more general view, corrugated $^{1}_{\infty}$[TGe] ribbons appear as part of two- or three-dimensional networks in various transition metal (T) germanides. For example, corrugated and parallel-oriented $^{1}_{\infty}$[TGe] ribbons are also found in $Sm_3Co_2Ge_4$ in which $^{1}_{\infty}$[CoGe] ribbons are interconnected via parallel-oriented $^{1}_{\infty}$[Ge] zigzag chains resulting in a [$CoGe_2$] layer (Supporting Information, Figure S4a).[38] In the structures of $Re_4Ni_2InGe_4$ (Re = Dy, Ho, Er, Tm) the connections between parallel-oriented $^{1}_{\infty}$[NiGe] ribbons are accomplished by $^{1}_{\infty}$[Ge_2In] zigzag chains (Supporting Information, Figure S4b).[39] In monoclinic YbFeGe $^{1}_{\infty}$[FeGe] ribbons occur. These ribbons are connected by Ge−Ge bonds forming $^{2}_{\infty}$[FeGe] layers (Supporting Information, Figure S4c).[40] In $Lu_3Ir_2Ge_3$ and Yb_2IrGe_2 such layers of Ge−Ge-connected $^{1}_{\infty}$[TGe] ribbons are further connected by bridging Ge atoms and Ge_2 dumbbells, respectively, into three-dimensional T−Ge frameworks (Supporting Information, Figure S4d,e).[41]

Chains composed solely of nickel and germanium atoms are also found as building blocks in other rare earth nickel germanides. Equimolar composition of the Ni−Ge polymers is retained also with other topology: Two different types of chains as well as isolated Ge atoms are found in $La_{11}Ni_4Ge_6$.[30] Ni−Ni edge-sharing Ni_4Ge_2 hexagons form planar $^{1}_{\infty}$[Ni_2Ge_2] bands, whereas the second polymeric unit builds planar polyacetylene-type $^{1}_{\infty}$[Ni] zigzag chains with *exo*-bonded Ge atoms (Figure 4a−c). Finally, La_3NiGe_2 possesses a similar heteroatomic planar polyacetylene-type $^{1}_{\infty}$[NiGe] zigzag chain with syntactic oriented Ge atoms bound to the Ni atoms (Figure 4d,e).[30] The formal addition of a further Ni atom, as shown in Figure 4f, leads to the topology of the ribbons of the title compounds. Thus, the polymer in La_3NiGe_2 can be seen as defective variant of the $^{1}_{\infty}$[NiGe] ribbons of Ba(Sr)NiGe.

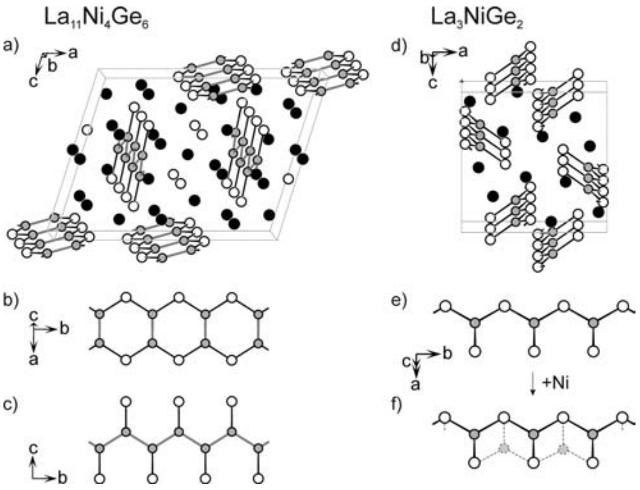

Figure 4. Crystal structure of $La_{11}Ni_4Ge_6$ (a) with one-dimensional polymorphic $^{1}_{\infty}$[NiGe] ribbons (b and c). Crystal structure of La_3NiGe_2 containing (d) $^{1}_{\infty}$[$NiGe_2$] chains (e), which are a defective variant of the $^{1}_{\infty}$[NiGe] ribbon (f) of Sr(Ba)NiGe. The Ni, Ge, and La atoms are drawn in gray, white, and black, respectively.

There also exist interesting similarities between equiatomic alkaline earth nickel germanides and their lead or tin halide prototypes. Although MgNiGe (TiNiSi-type structure, $PbCl_2$ binary prototype) and Sr(Ba)NiGe (anti-SnFCl-type structure) crystallize in the same space group *Pnma*, and the respective atoms occupy the same Wyckoff sites, they show an isopointal rather than an isotypic relationship, due to the significant differences in chemical bonding. The recently published CaNiGe[11] crystallizes in the CeFeSi- (or anti-PbFCl-) type structure (space group *P*4/*nmm*).

The halide $PbCl_2$ (binary prototype of the TiNiSi structure in which MgNiGe crystallizes)[42] topologically contains a three-dimensional $^{3}_{\infty}$[PbCl]$^{+}$ network (Supporting Information, Figure S5a) similar to the [NiGe]$^{2-}$ polyanionic network of MgNiGe. However, in the isoelectronic PbFCl-type structure $^{2}_{\infty}$[PbF]$^{+}$ layers with PbO-like topology are present,[30] which correspond to the [NiGe]$^{2-}$ polyanionic layers in CaNiGe (Supporting Information, Figure S5b). Furthermore, in the SnFCl-type structure (Supporting Information, Figure S5c),[43] which can be considered as the prototype of Sr(Ba)NiGe, topologically the one-dimensional $^{1}_{\infty}$[SnF]$^{+}$ ribbons can be found in analogy to the polyanionic [NiGe]$^{2-}$ ribbons of Sr(Ba)NiGe. Thus, most probably the size of the involved atoms plays a major role in the structure of the halides; however, in contrast to intermetallic phases, it affects the atomic positions of withthe "polycationic" units.

Magnetic Properties. The temperature dependence of the molar magnetic susceptibility χ_{mol} for SrNiGe and BaNiGe in the range 1.8−300 K is presented in Figure S6 (Supporting Information). The raw magnetization data were converted into molar magnetic susceptibilities (χ_{mol}'s) and subsequently corrected for the holder and for the diamagnetic contribution of the core electrons. For both compounds neither indications of superconductivity nor long-range magnetic ordering were observed down to a temperature of 1.8 K. Above 50 K the susceptibility of BaNiGe almost followed paramagnetic Curie−Weiss behavior, where local moments are supposed to arise probably from unpaired d-electrons of nickel, taking into account the unusual coordination of the Ni atoms. Fitting of the inverse magnetic susceptibilities using the Curie−Weiss law results in an effective magnetic moment $\mu_{eff} = 1.40(1)\ \mu_B$ per Ni atom in BaNiGe. Compared to the theoretical value for Ni^{2+} (2.83 μ_B) the obtained magnetic moments are rather small, which, along with the extremely high negative $\theta_c = -694$ K, might indicate the presence of short-range antiferromagnetic order at low temperatures, typical for low-dimensional magnets. For SrNiGe the plots of the inverse magnetic susceptibilities have a nonlinear trend, and at high temperatures they are almost temperature independent.

The temperature dependence of both the field-cooled (FC) and the zerofield-cooled (ZFC) magnetic susceptibility data for SrNiGe and BaNiGe at 50 Oe is shown in Figure S6 (insets, Supporting Information). The deviation of the FC and ZFC data for BaNiGe may be attributed to a minor trace of ferromagnetic impurities (most likely elemental nickel), although the powder diffractogram showed a single-phase BaNiGe sample. The pronounced irreversibility between the ZFC and FC susceptibilities and the presence of a broad cusp in the ZFC data at 14 K for SrNiGe is evidence for short-range magnetic ordering and can be associated with a spin-glass-like behavior. Such spin-glass behavior is also observed in other Ni-containing compounds with Ni as the only possible magnetic center.[44] Nevertheless, further investigations such as specific heat and electrical resistivity are needed for an unambiguous confirmation of the spin-glass-like behavior preferably on oriented single crystals to avoid the influence of impurities.

The magnetic susceptibility measurements in FC-ZFC mode for the MgNiGe sample, containing $MgNi_6Ge_6$ and Mg_2Ge as impurities, reveal no indications of superconductivity down to a temperature of 1.8 K (not shown here).

Electronic Structure Calculations. TB-LMTO-ASA electronic structure calculations were carried out for MgNiGe, CaNiGe, SrNiGe, and BaNiGe. In order to examine the electronic structure in detail and to compare the chemical bonding, the partial DOS, the band structures including fatbands, and the COHP and ELF have been calculated.

In all four equiatomic compounds MgNiGe, CaNiGe, SrNiGe, and BaNiGe, the alkaline earth metal atoms are the most eletropositive components (Pauling's electronegativities are 1.3 for Mg, 1.0 for Ca, 1.0 for Sr, 0.9 for Ba, 1.9 for Ni, and 2.0 for Ge). Thus, it can be assumed that the Ae atoms have largely transferred their valence electrons to the [NiGe] network, and to a first approximation the formula may be written as $Ae^{2+}[NiGe]^{2-}$, emphasizing the covalent Ni−Ge bonding within the polyanion. Although the description by a polyanionic network seems adequate at first sight, some words of caution seem to be appropriate, since significant bonding interactions also occur between the alkaline earth metal and the [NiGe] network. Especially, the shorter Mg−Ni and Mg−Ge interactions need to be considered (Table 3).

The calculated total and partial density of states (DOS) curves for MgNiGe, CaNiGe, SrNiGe, and BaNiGe are shown in Figures 5 and S7 (Supporting Information). For all compounds a nonzero value of the DOS is observed at E_F, thus indicating metallic conductivity. The total DOS curves of all four compounds can be divided in three parts. The first part (below −8 eV) has mainly Ge(s) character with minor contributions of Mg(s), Mg(p) or Ae(d) (Ae = Ca, Sr, Ba), and Ni(d) orbitals. The second part (approximately from −6.5 to −4 eV for MgNiGe and from −5 to −3 eV for other AeNiGe) is dominated by the Ge(p) and the Mg(s) and Mg(p) orbitals, and the third part of the total DOS curve (above −4 eV for MgNiGe and above −3 eV for other AeNiGe) is mainly dominated by the Ni(d) orbitals. The calculated integrated density of states of the Ni(d) orbitals in SrNiGe and BaNiGe indicates that they are not completely filled and have 8.6 electrons/atom at the Fermi level. Furthermore, the local maxima at the Fermi level in SrNiGe and BaNiGe, formed predominantly by Ni(d) states, can be correlated to a certain degree of structural or magnetic instability.

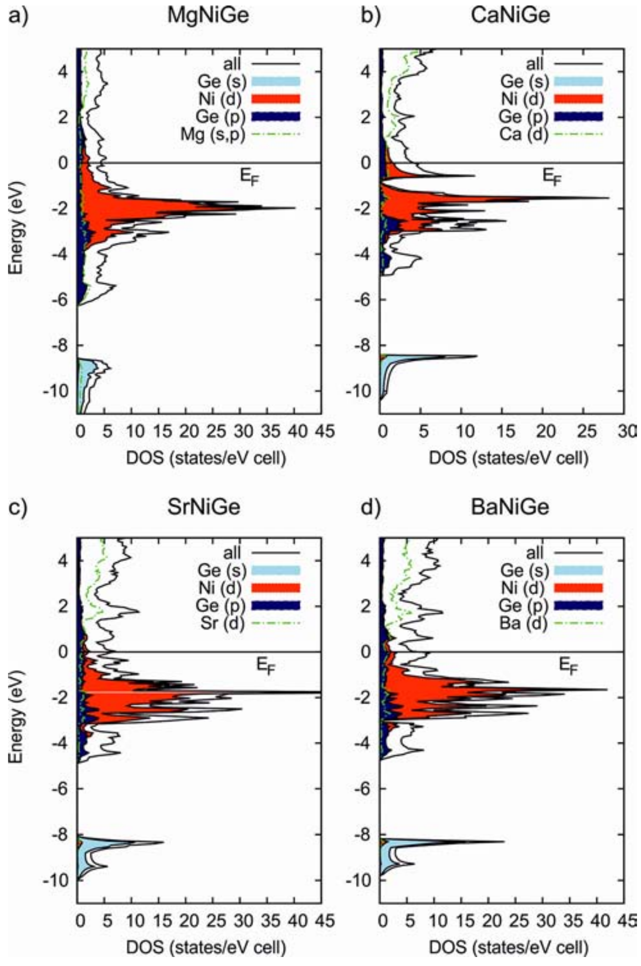

Figure 5. Total and partial DOS representations for MgNiGe (a), CaNiGe (b), SrNiGe (c), and BaNiGe (d). The energy zero is taken at the Fermi level E_F.

In the first part of the total DOS curves (below −8 eV) for CaNiGe, SrNiGe, and BaNiGe, a sharp peak is observed (Figures 5b−d), whereas for MgNiGe the DOS in the Ge(s) orbital region is rather flat (Figure 5a). This is in good agreement with the coordination pattern of the respective Ge atoms: in SrNiGe and BaNiGe the Ge atoms have three nearest Ni neighbors, and in CaNiGe the Ge atoms are situated on the tops of a $GeNi_4$ square pyramid and contain free electron pairs (lone pairs) with an orientation toward the electropositive Ca atoms,[11] whereas in MgNiGe the Ge atoms are tetrahedrally coordinated by Ni atoms. For MgNiGe, the flat DOS below −8 eV indicates steep bands and thus strong bonding interactions involving the Ge atoms. Similar curve progressions have been reported recently for the partial DOS of the E(s) (E = Ge, Si) orbitals of $CaNi_2Ge_2$ and $CaCo_2Si_2$: a flat DOS and thus steep bands are in accordance with the short E−E bonds between the $[T_2E_2]$ layers and correspond to a more regular coordination geometry of Ge atoms.[11,45] On the other hand a sharp partial DOS peak and thus flat bands have been described for the Ge(s) orbitals of $BaCo_2Ge_2$ and CaNiGe.[11,45] In these structures there exist no Ge−Ge contacts between similar layers, and consequently, lone pairs are located at the Ge atoms, which are responsible for the flat band sections in the electronic band structure and for the corresponding sharp DOS peak.[46]

In BaNiGe the narrow band gap of 0.07 eV separates the second and third part of the DOS around −3.1 eV. In MgNiGe, CaNiGe, and SrNiGe, this gap is absent. However, for CaNiGe a pseudogap of 0.1 eV is observed at about −0.8 eV.

Figures 6 and S8−S11 (Supporting Information) show the band structures including fatbands for MgNiGe, CaNiGe, SrNiGe, and BaNiGe. The difference between the three-dimensional MgNiGe structure and the structure of Sr(Ba)-NiGe with one-dimensional motifs becomes obvious at first sight. In the band structure of MgNiGe a band crossing is observed around E_F. In contrast, for SrNiGe the bands below and above the Fermi level (valence and conduction bands, respectively) do not mix together and are energetically separated for all k points, but cross the Fermi level. This situation is typically observed for semimetals. Similarly, such a separation of bands is observed for BaNiGe; however, in this case valence and conduction bands touch each other at Γ at +0.4 eV. The separation of bands is due to an "avoided crossing" of the bands, which takes place for both SrNiGe and BaNiGe. In order to allow a comparison with the band structure of CaNiGe, a band path comparable to the one used for MgNiGe, SrNiGe, and BaNiGe has been chosen. Taking into account that the symmetry reduction from CaNiGe (*P*4/*mmn*) to Sr(Ba)NiGe (*Pnma*) might lead to an avoidance of a

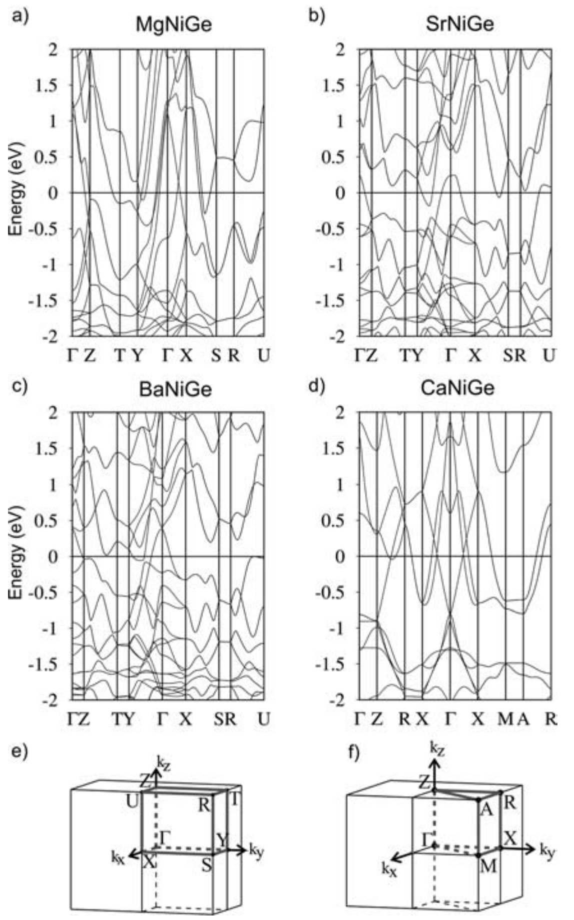

Figure 6. Band structures for MgNiGe (a), SrNiGe (b), BaNiGe (c), and CaNiGe (d) in the range from −2 to 2 eV. The symmetry points in *k* space are given according to the Brillouin zone with respect to the reciprocal conventional vectors, (e) for space group *Pnma* (MgNiGe, SrNiGe and BaNiGe), (f) for space group *P4/nmm* (CaNiGe).

crossing of bands, similarities between the band structures become visible. For example, for CaNiGe the bands touch at Γ at −0.8 eV. This corresponds to the avoided crossing of bands at Γ at +0.4 eV for BaNiGe. Otherwise valence and conduction bands do not cross. As the inter-ribbon distances of the $^1_\infty$[NiGe] ribbons are shorter for SrNiGe than for BaNiGe, the separation of the bands is more pronounced. In the band structures of SrNiGe and BaNiGe the avoided crossings next to E_F are further displayed in the local maximum at E_F of the corresponding DOS (Figures 5c,d). No flat bands are observed here. As to be expected for the crystal structure of CaNiGe with two-dimensional structure motifs, no bands crossing E_F in the sections parallel to the *c* axis Γ → Z and M → A are observed. However, one band crosses E_F in the section R → X, which corresponds to the same crystallographic direction. The analysis of the fatbands reveals that the orbitals Ca d_{yz}, Ni d_{yz}, and Ni d_{z^2} contribute to this band. This underlines a weak interaction of the Ca atoms with the $^2_\infty$[NiGe] layers.

For a more quantitative bond analysis a crystal orbital Hamilton population analysis was carried out (COHP) which provides a quantitative measure of the strength of the chemical bonds. COHP curves for selected interactions are shown in Figures 7 and S12−S16 (Supporting Information), and the calculated integrated −iCOHP values are given in Table 3. The strongest bonding interactions (i.e., −iCOHP values) were found for the shortest Ni−Ge contacts of the title compounds (Figure 7). For all Ni−Ge contacts a bonding character is found up to the Fermi level. The maxima of the −iCOHP curves clearly reveal that the Ni−Ge bonds for SrNiGe (2.308 Å) and BaNiGe (2.317 Å) are optimized at the Fermi level: Ni−Ge bonding states are filled, and antibonding ones are empty (Figure 7c,d). Similarly, an optimized Ni−Ge bond (2.341 Å) is found in $CaNiGe_2$[7] and a Co−Ge bond (2.290 Å) in $SrCo_{5-x}Ge_9$.[47] In contrast, for the Ni−Ni contacts in MgNiGe, CaNiGe, SrNiGe, and BaNiGe bonding as well as antibonding interactions are observed below E_F (see Supporting Information, Figure S12). The COHP curves for the Ae−Ni contacts are given in Figures S13−S16 (Supporting Information). They mostly display bonding interactions in the region directly above E_F. Considering the Ae−Ni interactions, the calculated −iCOHP values reveal that interactions between the cations (Ae^{2+}) and the [NiGe] framework in MgNiGe are significantly stronger compared to those in CaNiGe and Sr(Ba)NiGe. The −iCOHP values are in good accordance with those of other recently published Ni-rich Ae/Ni/Ge compounds.[5,12−15]

Further insight into the nature of the bonding is provided by the electron localization function (ELF), sketched in Figure 8. The ELF of BaNiGe has the same general features as those of SrNiGe, and is therefore not discussed. Even though high −iCOHP values are observed for the short Ni−Ge contacts, no disynaptic valence basins are detected. This is a common feature found for various compounds of the systems Ae/Ni/Ge.[11−15] In MgNiGe one valence basin ① is observed next to the Ge atoms (Figure 8a). As the four nearest Ni neighbors of the Ge atom are arranged in a close trigonal-pyramidal (or tetrahedral) coordination with the Ge atom located close to the basal plane, a large free space results next to the Ge atom. This valence basin ① is directed toward the neighboring Mg atoms and consists of three maxima which appear below $\eta = 0.58$. For CaNiGe (Figure 8b) one valence basin ② is observed next to the Ge atoms. It consists of one maximum which is directed toward the nearest Ca atom and appears below $\eta = 0.78$. For SrNiGe (Figure 8c) one monosynaptic valence basin ③ at $\eta = 0.73$ corresponds to the lone pair of the Ge atom and is oriented in between two neighboring Sr atoms. The valence basin at the Ge atom in the MgNiGe structure is less pronounced than those in CaNiGe and SrNiGe, which is reflected in the electronic band structure discussed before.

CONCLUSION

The size restrictions implied by the alkaline earth elements Mg, Ca, Sr, and Ba lead to interesting features in the equiatomic AeNiGe compounds. With the smallest alkaline earth metal magnesium, MgNiGe (TiNiSi type) with a three-dimensional $^3_\infty$[NiGe] polyanionic network is formed; CaNiGe crystallizes in the well-known CeFeSi type with PbO-like $^2_\infty$[NiGe] layers, whereas the large Sr and Ba cations lead to the formation of structures with one-dimensional $^1_\infty$[NiGe] ribbons. Such one-dimensional polyanions are unique in the crystal chemistry of polar intermetallic compounds but are the main building blocks of many transition metals germanides. The substitution of large cations by the smaller ones (Ba−Sr−Ca−Mg) step by step leads to a compression of the structure, which can be understood as a “chemical pressure effect”. Therefore, the series of equiatomic compounds AeNiGe (Ae = Mg, Ca, Sr, Ba) are excellent examples for the influence of the Ae cation size on the dimensionality of the polyanions.

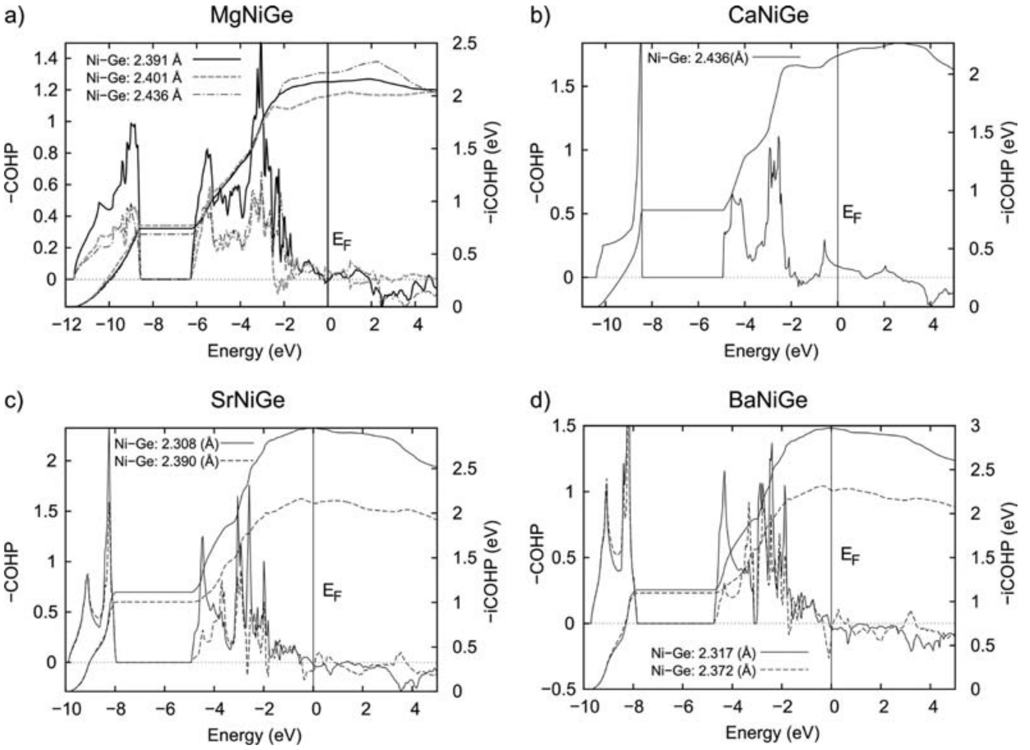

Figure 7. Crystal orbital Hamilton population (COHP) and integrated crystal orbital Hamilton population (−iCOHP) curves for corresponding Ni−Ge bonds within the [NiGe] substructure of MgNiGe (a), CaNiGe (b), SrNiGe (c), and BaNiGe (d).

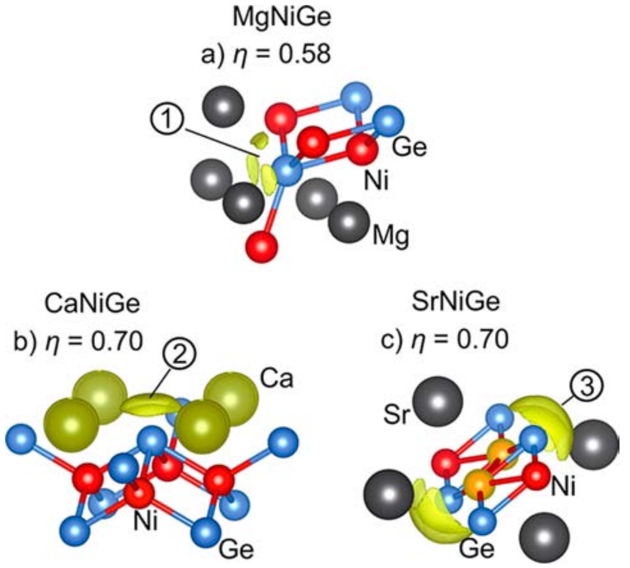

Figure 8. Three-dimensional ELF plots with (a) isosurface at $\eta(r)$ = 0.58 for MgNiGe, (b) isosurface at $\eta(r)$ = 0.70 for CaNiGe, and (c) isosurface at $\eta(r)$ = 0.70 for SrNiGe.

It is tempting to associate the structure to an electronic scheme according to Zintl as $Ae^{2+}Ni^{2+}Ge^{4-}$. However, the small differences in the electronegativities of Ni and Ge, as well as the existence of significant Ni−Ge interactions, dispute this simple assignment. It is more appropriate to depict the [NiGe] infinite ribbon, layer, and network as $[NiGe]^{2-}$ polyanions. Our investigations of Ae/Ni/Ge systems showed that the CeFeSi-type structure is structurally less stable toward an Ae exchange in comparison to the $ThCr_2Si_2$-type structure with the same PbO-type [NiGe] layers.[4,9,16] Nevertheless, other equiatomic alkaline earth transition metal germanides SrMnGe and BaMnGe[48] with larger cations, as well as MgCuGe[49] and the recently described MgCoGe[11] with smaller cations, adopt the same tetragonal CeFeSi-type structure with polyanionic layers comparable to those in CaNiGe. Equiatomic rare earth metal nickel germanides crystallize with orthorhombic TiNiSi- (or $CeCu_2$-) type structure with three-dimentional polyanionic networks,[30,50] whereas EuNiGe (isoelectronic to AeNiGe) adopts the monoclinic $CoSb_2$-type structure with polyanionic layers.[51,52] All these facts of structural diversity suggest that the formation of the structure types depends on the size of the involved atoms and also on the valence electron concentration. Further, polymorphism can occur as it has been observed for other 1:1:1 germanides such as CaAuGe,[53] LuNiGe,[54] and RePdGe (Re = heavy rare earth elements).[55]

Furthermore, the existence of isolated $^{1}_{\infty}$[NiGe] ribbons in Sr(Ba)NiGe as well as their prevalence in other intermetallic compounds opens the possibility of using such building blocks as precursors for new composite materials.

■ ASSOCIATED CONTENT

Ⓢ Supporting Information

Detailed crystallographic data of crystals MgNiGe, SrNiGe, and BaNiGe in CIF format. Figures of powder X-ray patterns of MgNiGe, SrNiGe, and BaNiGe (Figures S1−S3); the structures of other transition metal germanides containing $^{1}_{\infty}$[TGe] ribbons (Figure S4); the structures of $PbCl_2$, PbFCl, and SnFCl (Figure S5); the temperature dependence of the magnetic susceptibility of BaNiGe and SrNiGe (Figure S6); partial DOS curves for the alkaline earth metal s, p, and d orbitals of AeNiGe (Ae = Mg, Ca, Sr, Ba) (Figure S7); band structures including fatbands of AeNiGe (Ae = Mg, Ca, Sr, Ba) (Figures S8−S11); COHP of the Ni−Ni, Ae−Ni, and Ae−Ge interaction for AeNiGe (Ae = Mg, Ca, Sr, Ba) (Figures S12−

S16). This material is available free of charge via the Internet at http://pubs.acs.org.

AUTHOR INFORMATION

Corresponding Author

*E-mail: thomas.faessler@lrz.tu-muenchen.de.

Notes

The authors declare no competing financial interest.

ACKNOWLEDGMENTS

This research was supported by the Deutsche Forschungsgemeinschaft within the priority program SPP-1458 (Project HL 62/1-1).

REFERENCES

(1) Nesper, R. *Angew. Chem., Int. Ed. Engl.* **1991**, *30*, 789−817.

(2) Buchholz, W.; Schuster, H. U. *Z. Anorg. Allg. Chem.* **1981**, *482*, 40−48.

(3) Markiv, V. Y.; Teslyuk, M. Y.; Gladyhevskii, E. I. *Dopov. Akad. Nauk Ukr. RSR* **1964**, *7*, 914−916.

(4) Bodak, O. I.; Gladyshevskii, E. I. *Dopov. Akad. Nauk. Ukr. RSR* **1968**, *30*, 944−947.

(5) Siggelkow, L.; Hlukhyy, V.; Wahl, B.; Fässler, T. F. *Eur. J. Inorg. Chem.* **2011**, 4012−4024.

(6) Hlukhyy, V.; Fässler, T. F. In *GDCh-Jahrestagung*; Düsseldorf, Germany, 2005; p Mat020.

(7) Hlukhyy, V.; Eck, S.; Fässler, T. F. *Inorg. Chem.* **2006**, *45*, 7408−7416.

(8) Hlukhyy, V.; Siggelkow, L.; Fässler, T. F. *Z. Anorg. Allg. Chem.* **2012**, *638*, 2029−2034.

(9) Dörrscheidt, W.; Niess, N.; Schäfer, H. *Z. Naturforsch.* **1976**, *B31*, 890−891.

(10) Nguyen, L. T. K.; Aydemir, U.; Baitinger, M.; Bauer, E.; Borrmann, H.; Burkhardt, U.; Custers, J.; Haghighirad, A.; Hofler, R.; Luther, K. D.; Ritter, F.; Assmus, W.; Grin, Y.; Paschen, S. *Dalton Trans.* **2010**, *39*, 1071−1077.

(11) Hlukhyy, V.; Chumalo, N.; Zaremba, V.; Fässler, T. F. *Z. Anorg. Allg. Chem.* **2008**, *634*, 1249−1255.

(12) Hlukhyy, V.; Fässler, T. F. *Z. Anorg. Allg. Chem.* **2010**, *636*, 100−107.

(13) Siggelkow, L.; Hlukhyy, V.; Fässler, T. F. *Z. Anorg. Allg. Chem.* **2010**, *636*, 1870−1879.

(14) Hlukhyy, V.; Fässler, T. F. *Z. Anorg. Allg. Chem.* **2008**, *634*, 2316−2322.

(15) Siggelkow, L.; Hlukhyy, V.; Fässler, T. F. *Z. Anorg. Allg. Chem.* **2011**, *637*, 2000−2006.

(16) Hlukhyy, V.; Senyshyn, A.; Trots, D.; Fässler, T. F. *HASYLAB Ann. Rep.* **2007**, *1*, 1021−1022.

(17) Liu, X.; Matsuishi, S.; Fujitsu, S.; Hosono, H. *Phys. Rev. B* **2011**, *84*, 214439.

(18) Liu, X.; Matsuishi, S.; Fujitsu, S.; Ishigaki, T.; Kamiyama, T.; Hosono, H. *J. Am. Chem. Soc.* **2012**, *134*, 11687−11694.

(19) Rodriguez-Carvajal, J. *Physica B* **1993**, *192*, 55−69.

(20) Busch, G.; Winkler, U. *Physica* **1954**, *20*, 1067−1072.

(21) *X-SHAPE Version 2.11*; STOE & Cie GmbH: Darmstadt, Germany, 2008.

(22) *X-RED32 Version 1.48*; STOE & Cie GmbH: Darmstadt, Germany, 2008.

(23) *SCALE3 ABSPACK: Empirical Absorption Correction*; Oxford Diffraction Ltd.: Oxford, 2006.

(24) Sheldrick, G. M. *SHELXS-97−Program for the Determination of Crystal Structure*; University of Göttingen: Göttingen, Germany, 1997.

(25) Sheldrick, G. M. *SHELXL-97−Program for Crystal Structure Refinement*; University of Göttingen: Göttingen Germany, 1997.

(26) Schilfgarde, M. v.; Paxton, T. A.; Jepsen, O.; Andersen, O. K.; Krier, G. *TB-LMTO-ASA Version 4.7*; Max-Planck-Institut für Festkörperforschung: Stuttgart, Germany, 1998.

(27) Lambrecht, W. R. L.; Andersen, O. K. *Phys. Rev. B* **1986**, *34*, 2439−2449.

(28) Andersen, O. K.; Jepsen, O. *Phys. Rev. Lett.* **1984**, *53*, 2571−2574.

(29) Dronskowski, R.; Blochl, P. E. *J. Phys. Chem.* **1993**, *97*, 8617−8624.

(30) *Inorganic Crystal Structure Database (on CD-Rom), Version 1.4.6*; Fachinformationszentrum: Karlsruhe, Germany, 2009.

(31) Landrum, G. A.; Hoffmann, R.; Evers, J.; Boysen, H. *Inorg. Chem.* **1998**, *37*, 5754−5763.

(32) Hoffmann, R.-D.; Pöttgen, R. *Z. Kristallogr.* **2001**, *216*, 127−145.

(33) Pauling, L.; Kamb, B. *Proc. Natl. Acad. Sci. U.S.A.* **1986**, *83*, 3569−3571.

(34) Nuspl, G.; Polborn, K.; Evers, J.; Landrum, G. A.; Hoffmann, R. *Inorg. Chem.* **1996**, *35*, 6922−6932.

(35) Pöttgen, R.; Johrendt, D. *Chem. Mater.* **2000**, *12*, 875−897.

(36) Overberger, C.; Moore, J. In *Advances in Polymer Science*; Springer: Berlin, 1970; Vol. 7, pp 113−150.

(37) Sofo, J. O.; Chaudhari, A. S.; Barber, G. D. *Phys. Rev. B* **2007**, *75*, 153401.

(38) Mruz, O. Y.; Fedyna, M. F.; Pecharskii, V. K.; Bodak, O. I. *Inorg. Mater.* **1989**, *25*, 1708−1710.

(39) Salvador, J. R.; Kanatzidis, M. G. *Inorg. Chem.* **2006**, *45*, 7091−7099.

(40) Sologub, O.; Salamakha, P.; Bocelli, G.; Otani, S.; Takabatake, T. *J. Alloys Compd.* **2000**, *312*, 196−200.

(41) Rodewald, U. C.; Pottgen, R. *Solid State Sci.* **2003**, *5*, 487−493.

(42) Sahl, K.; Zemann, J. *Naturwissenschaften* **1961**, *48*, 641−642.

(43) Geneys, C.; Vilminot, S.; Cot, L. *Acta Crystallogr.* **1976**, *B 32*, 3199−3202.

(44) Liao, C. Z.; Dong, C.; Zeng, L. M.; He, B.; Cao, W. H.; Yang, L. H. *J. Alloys Compd.* **2010**, *493*, 31−34.

(45) Siggelkow, L.; Hlukhyy, V.; Fässler, T. F. *Z. Anorg. Allg. Chem.* **2010**, *636*, 378−384.

(46) Fässler, T. F. *Chem. Soc. Rev.* **2003**, *32*, 80−86.

(47) Hlukhyy, V.; Fässler, T. F.; Claus, P. *Z. Anorg. Allg. Chem.* **2009**, *635*, 708−716.

(48) Dascoulidou, A.; Müller, P.; Bronger, W. *Z. Anorg. Allg. Chem.* **1998**, *624*, 124−128.

(49) Schuster, H. U.; Bockelmann, W.; Captuller, J. *Z. Naturforsch.* **1970**, *B25*, 1303.

(50) Villars, P.; Cenzual, K. *Pearson's Crystal Data−Crystal Structure Database for Inorganic Compounds (on CD-ROM)*; ASM International: Materials Park, Ohio, 2012/13.

(51) Pöttgen, R. *Z. Naturforsch.* **1995**, *B50*, 1181−1184.

(52) Oniskovets, B. D.; Belsky, V. K.; Pecharsky, V. K.; Bodak, O. I. *Kristallografiya* **1987**, 32, 888−890.

(53) Merlo, F.; Pani, M.; Canepa, F.; Fornasini, M. L. *J. Alloys Compd.* **1998**, *264*, 82−88.

(54) Koterlyn, G. M.; Bodak, O. I.; Pavlyuk, V. V.; Stepien-Damm, J.; Pietraszko, A. *J. Alloys Compd.* **1999**, *291*, 110−116.

(55) Rodewald, U. C.; Heying, B.; Hoffmann, R.-D.; Niepmann, D.; Poettgen, R. *Z. Naturforsch., B* **2009**, *64*, 595−602.